Under Review in Marine Pollution Bulletin (July, 2021)

Pre- and post-industrial levels of polycyclic aromatic hydrocarbons in sediments from the Estuary and Gulf of St. Lawrence (eastern Canada)

Anne Corminboeuf [1, *], Jean-Carlos Montero-Serrano [1,*], Richard St-Louis [2], Allyson Dalpé [1,2,3], Yves Gélinas [4]

[1] Institut des sciences de la mer de Rimouski, Université du Québec à Rimouski, 310 Allée des Ursulines, Rimouski, QC, G5L 3A1, Canada

[2] Université du Québec à Rimouski, 300 Allée des Ursulines, Rimouski, QC, G5L 3A1, Canada

[3] Département de Chimie, Université Laval, Pavillon Alexandre-Vachon, 1045 avenue de la Médecine, Université Laval, Québec, QC, G1V 0A6, Canada

[4] Geotop and Department of Chemistry and Biochemistry, Concordia University, 7141 Sherbrooke St. West, Montréal, Québec H4B 1R6, Canada

* Corresponding authors: A. Corminboeuf (annecorminboeuf@hotmail.com) and J.-C. Montero-Serrano (jeancarlos_monteroserrano@uqar.ca)

Highlights

- The PAH contents are similar to those in other well-urbanized estuarine systems.
- The PAH contents between 1937 and 1943 CE are 2.5 times higher than modern values.
- PAHs mainly originate from pyrogenic sources with little petrogenic influence.
- A few urbanized sector samples exhibit a possible ecological risk to organisms.

Abstract

The concentrations of 23 polycyclic aromatic hydrocarbons (PAHs; 16 parent PAHs and 7 alkyl-PAHs) were determined in 45 surface sediment and 7 basal sediment box core samples retrieved from the Estuary and Gulf of St. Lawrence in eastern Canada. The concentration sums of 16 priority PAHs (Σ_{16}PAHs) in the surface sediments ranged from 71 to 5672 ng g^{-1}. Σ_{16}PAHs in the basal sediments ranged from 93 to 172 ng g^{-1} among the pre-industrial samples and from 1216 to 1621 ng g^{-1} among the early post-industrial samples. The highest Σ_{16}PAH values occurred in samples retrieved from the Baie-Comeau-Matane area, an area affected by intense industrial anthropogenic activities.

Source-diagnostic PAH ratios suggest a predominance of pyrogenic sources via atmospheric deposition, with a minor contribution of petrogenic seabed pockmark sources. The PAH concentrations in the sediments from the study areas reveal low ecological risks to benthic or other organisms living near the water-sediment interface.

Keywords: St. Lawrence Estuary, sediments, polycyclic aromatic hydrocarbons, baseline, risk assessment, spatial distribution.

The St. Lawrence River and Estuary System, located in eastern Canada, originates in the Great Lakes and flows along a distance of more than 3200 km until reaching the Cabot Strait and Atlantic Ocean (Government of Canada, 2017). With a hydrological basin of more than 1 million km^2, it ranks among the largest rivers in North America (El Sabh and Silverberg, 1990; Camu *et al*. 2019). This large estuarine system is generally divided into three regions with distinct oceanographical features, i.e., the Upper Estuary, Lower Estuary and Gulf of St. Lawrence (Fig. 1; El Sabh and Silverberg, 1990). This system is as wide as 50 km and as deep as ~ 350 m at its center, where a depression is formed, namely, the Laurentian Channel (Loring and Nota, 1973; Normandeau *et al.*, 2015). Moreover, this system is a major international trade route connecting eastern Canada to the Atlantic Ocean (Camu *et al*. 2019). In 2017, shipments via the Great Lakes to the St. Lawrence Waterway System (i.e., from the Great Lakes to the St. Lawrence Gulf) generated 59 billion dollars (CAD) through economic activities for Canada and the United States (Martin Associates, 2018). This system is also the main route for the transit of 231 million metric tons of cargo and directly supports more than 105000 U.S. and Canadian jobs (Martin Associates, 2018). Approximately 4000 vessels travel along this seaway every year, transporting mainly agricultural, mining and manufactured products (St. Lawrence Seaway Corporation Management, 2019). More than 15 million Canadians reside in the hydrographic system of St. Lawrence, who have contributed, combined with industrial activities, to past and present anthropogenic stress levels in regard to many pollutants, including polycyclic aromatic hydrocarbons (PAHs; Government of Canada, 1994).

PAHs constitute a wide class of organic pollutants comprising fused benzene rings (Haritash and Kaushik, 2009; AMAP, 2017). In the 1970s, 16 PAHs mainly emitted during fuel combustion were listed as priority environmental pollutants by the Environmental

Protection Agency of the United States (US EPA) and Government of Canada (Meek *et al.,* 1994; Keith, 2014; AMAP, 2017; Roslund *et al.,* 2018). Pyrogenic PAHs are produced via incomplete organic matter combustion (e.g., forest fires, volcanic eruptions and fossil fuel burning), while petrogenic PAHs are introduced into aquatic systems via natural oil seeps, accidental oil spills and rock weathering (Lima *et al.,* 2005; Pampanin and Sydnes, 2017; Chen *et al.,* 2018; Yu *et al.,* 2019). PAHs are therefore derived from either natural processes or anthropogenic sources, but anthropogenic activities are the predominant PAH sources in the environment (Yanik *et al.,* 2003; Morillo *et al.,* 2008). PAHs do not readily degrade under natural conditions, and they thus tend to be moderately persistent (Pelletier *et al.,* 2008; Haritash and Kaushik, 2009). Given their general low vapor pressure and hydrophobicity, PAHs typically accumulate in sediments, where they are ultimately trapped (Page *et al.,* 1999; Haritash and Kaushik, 2009; AMAP, 2017). Bioaccumulation of PAHs might occur in certain invertebrates, such as blue mussels, upon exposure, but most vertebrates can readily metabolize these substances (Xue et Warshawsky, 2005; Haritash and Kaushik, 2009; Klungsøyr *et al.,* 2010). The main concern arises from their carcinogenic/mutagenic potential during phase I metabolism in vertebrates (Van Schooten, 1991; Xue and Warshawsky, 2005; Haritash and Kaushik, 2009).

The aims of this baseline study are therefore to (1) assess the PAH distribution and level in modern sediments retrieved from the Estuary and Gulf of St. Lawrence (EGSL); (2) determine their origin (i.e., pyrogenic or petrogenic) via diagnostic ratios, and finally (3) compare PAH levels between surface (post-1900) and basal (pre-1900) sediment samples obtained from selected cores. To achieve these goals, a total of 45 surface sediment samples was collected in the EGSL, i.e., from Québec city in the riverine section of the St. Lawrence System to the Old Harry oil and gas field in the Gulf of St. Lawrence (Fig. 1), with a Van Veen grab sampler (14 samples) or a box corer (31 samples). The uppermost 1-cm sediment layer was recovered using a spatula and stored in plastic bags (WhirlPack) at 4°C until further analysis. In addition, 7 push cores were subsampled from a box core collected in the Upper Estuary and Gulf of St. Lawrence and stored at 4°C (Fig. 1). Once at the laboratory, these push cores were sampled at the bottom (the last cm of each core). High-resolution seismic profiles were considered to target coring sites where sediment accumulation was not influenced by mass wasting events (Montero-Serrano *et al.,* 2018,

2019, 2020a,b). All samples were retrieved during the 2018, 2019, and 2020 Odyssée St-Laurent winter expeditions (hereinafter referred to as AMD18-OSL, AMD19-OSL, and AMD20-OSL, respectively) onboard the Canadian Coast Guard Ship (CCGS) icebreaker Amundsen and the 2020 Québec Maritime Network (Réseau Québec Maritime or RQM)-Marine Environmental Observation Prediction and Response Network (MEOPAR) expedition onboard the research vessel (R/V) Coriolis II (hereinafter referred to as COR2001). As modern sedimentation rates in the EGSL diminish exponentially from ~0.50 – 0.74 cm yr^{-1} at the head of the estuary to 0.11–0.25 cm yr^{-1} in the gulf (Smith and Schafer, 1999; Muzuka and Hillaire-Marcel, 1999; St-Onge *et al.*, 2003; Barletta *et al.*, 2010; Genovesi *et al.*, 2011; Thibodeau *et al.*, 2013), we estimate that surface sediments correspond to modern times at the head of the estuary, and they correspond the last decade at most in the gulf.

In regard to PAH extraction, the samples were sieved through a 150-µm Nitex® mesh to avoid any influence related to grain size variability. The <150 µm fraction was freeze dried and crushed, and homogenized aliquots were employed for PAH extraction. All reagents were of analytical or high-performance liquid chromatography (HPLC) grade. PAHs were extracted via the one-step integrated accelerated solvent extraction (ASE) method developed by Choi *et al*. (2014) and implemented in other baseline studies targeting PAHs (e.g., Corminboeuf *et al.*, 2021). Copper powder (<425 µm), which was activated with hydrochloric acid (HCl) 6 N, was employed to remove elemental sulfur, after which the samples were shaken for 3 min, rinsed with distilled water until a neutral pH was attained and then rinsed 3 times with both methanol and dichloromethane. Two deuterated spikes, i.e., 1-methylnaphthalene and benz(a)anthracene, were directly added onto each sediment sample before the packed extraction cells were left unsealed and loosely covered for 2 h at room temperature (Fig. S1). One blank, one duplicate, and one standard reference material NIST-1944 (National Institute of Standards and Technology, Gaithersburg, MD, USA) were analyzed with every batch of samples (12 samples/batch) to assess the method precision and accuracy. The adopted Dionex ASE 200 system (Thermo CO., Sunyvale, CA, USA) was set to the following conditions: hexanes and dichloromethane were applied as the solvent (4:1 v/v) at a temperature of 100°C and pressure of 1700 psi, with a flush volume of 60%, a purge time of 100 s and two static

cycles of 5 min. With the use of a rotating evaporator, the extracts were evaporated to approximately 5 mL and then to exactly 0.5 mL under a nitrogen gas stream at room temperature. The obtained extracts were then analyzed using a gas chromatograph (Agilent Technologies 6850 series II) coupled to a mass spectrometer (Agilent Technologies 5975B VL MSD). Splitless injection of 1 µL was performed with an autosampler (Agilent Technologies Auto Sampler 6850 series) with helium as the carrier gas at a flow rate of 1 mL min^{-1}. An Rxi®-5ms capillary column (30 m x 0.25 mm inner diameter (ID) x 0.25 µm FT, 5% diphenyl and 95% polysiloxane) was adopted. The oven temperature program was set as follows: 50°C for 2 min, 15°C/min until 275°C followed by a hold period of 2 min, 15°C/min until 325°C followed by a hold period 15 min, and a postrun of 2 min at 300°C. PAH Mix manufactured by AccuStandard was used to build calibration curves, together with a homemade alkylated PAH mix.

A total of 23 PAHs (the 16 priority PAHs identified by the US EPA and 7 alkyl-PAHS) was targeted in this study: naphthalene, 1-methylnaphthalene, 2-methylnaphthalene, 2,6-dimethylnaphthalene, acenaphthylene, acenaphthene, 2,3,5-trimethylnaphthalene, fluorene, phenanthrene, anthracene, 1-methylphenanthrene, 3,6-dimethylphenanthrene, fluoranthene, pyrene, 9,10-dimethylanthracene, benz(a)anthracene, chrysene, benzo(b)fluoranthene, benzo(k)fluoranthene, benzo(a)pyrene, indeno(1,2,3-c,d)pyrene, dibenz(a,h)anthracene and benzo(g,h,i)perylene. The PAH concentrations were not blank corrected since the detected contamination measured in the procedural blanks was below 0.01 µg mL^{-1} (Table S1). The spike recoveries were 45 ± 17% (n=55) for 1-methynaphthalene-d10 and 64 ± 27% (n=55) for benz(a)anthracene-d12, and the samples were hence all spike corrected. The recoveries for 1-methynaphthalene-d10 were used to correct the results obtained for the 15 first PAHs in the above list (from napthalene to 9,10-dimethyanthracene), and the recoveries for benz(a)anthracene-d12 were used to correct the results obtained for the remaining PAHs (from pyrene to benzo(g,h,i)perylene. The method detection limit (MDL) for each PAH was calculated as suggested by the US EPA (Oblinger Childress *et al.*, 1999). Thus, 7 replicates of the second-lowest calibration point were analyzed. The MDL was then obtained by multiplying the standard deviation of the determined concentration for each compound by 3.143. The MDL ranged from 1.6 ng g^{-1} for benz(a)anthracene to 31.2 ng

g^{-1} for acenaphthylene (Table S2). Diagnostic ratios of fluoranthene over the sum of fluoranthene and pyrene (Fla/[Fla+Pyr]) and of benz(a)anthracene over the sum of benz(a)anthracene and chrysene (BaA/[BaA+Chr]) were considered to discriminate PAH sources (i.e., pyrogenic vs petrogenic).

Sediment grain size analysis was performed on the <150 µm sediment fraction with a Beckman Coulter LS13320 laser particle size analyzer in regard to the AMD19-OSL samples, and a Malvern Panalytical Mastersizer 3000 was adopted to analyze the AMD18-OSL, AMD20-OSL and COR2001 samples. Prior to grain size analysis, all samples were treated with ~5 mL of hydrogen peroxide (H_2O_2) and ~5 mL of hydrochloric acid (HCl 1 M) and then rinsed 3 times with distilled water before the addition of ~20 mL of sodium hexametaphosphate.

The total carbon (TC) and total organic carbon (TOC) contents in the <150 µm sediment fraction were quantified at the Geotop Light Stable Isotope Geochemistry Laboratory (Montréal, Québec) with a Carlo-Erba NC 2500 elemental analyzer and following the acidification in solution method described in Hélie (2009). The analytical precision and accuracy were determined via duplicate sample analysis and replicate analyses of in-house and international standards (low-organic content soil, cyclohexanone-2,4-dinitrophenylhydrazone, atropine and acetanilide), respectively, and were better than ±0.02% (1σ).

Regarding data processing, we followed the approach presented in Corminboeuf *et al.* (2021) and used R software (R Core Team, 2021) to perform statistical analysis. Briefly, values below the detection limit were imputed via multiplicative lognormal replacement with the zCompositions package (Palarea-Albaladejo and Martin-Fernandez, 2015) to preserve the geometry of the compositional data while accounting for corresponding detection limit thresholds. A log-centered (clr) transform was applied to the data with the compositions package (van den Boogaart and Tolosana-Delgado, 2008) to allow the valid application of classical (Euclidean) statistical methods to the compositional data (Aitchison, 1986, 1990; Montero-Serrano *et al.*, 2010). The NbClust (Charrad *et al.*, 2014) and factoextra (Kassambara and Mundt, 2020) packages were employed to determine the optimum number of clusters. Samples possessing similar PAH compositions within the EGSL were identified via fuzzy c-means (FCM; Kaufman and Rousseeuw, 2009)

clustering analysis with the cluster package (Maechler *et al.*, 2019). The FCM clustering results were visualized through principal coordinate ordination and silhouette plots, which allow visualization of the robustness of clusters (Kaufman and Rousseeuw, 2009; Borcard *et al.*, 2011; Gamboa *et al.*, 2017). Principal component analysis (PCA) was performed of the PAH data and FCM clustering results with the goal of determining PAH associations with similar relative variation patterns (von Eynatten *et al.*, 2003; Montero-Serrano *et al.*, 2010). PCA was conducted with the compositions and factoextra packages. Finally, the FCM clustering results and TOC and Σ_{16}PAH data were employed to produce interpolated maps in Ocean Data View software (Schlitzer, 2021). These interpolated maps were generated using a weighted-average gridding algorithm with a quality limit of 1.2.

All analytical data presented are available electronically in Table S4. FCM clustering analysis revealed that there were two regional PAH clusters within the EGSL (hereinafter referred to as PAH C#1 and PAH C#2; Fig. 2A-C). PAH C#1 represents the samples collected in the Lower Estuary, mostly in the Baie-Comeau-Matane area (Fig. 2C), an area influenced by intense industrial anthropogenic activities (Pellerin-Massicotte, 1993; Working Group on the State of St. Lawrence Monitoring, 1994; Gagnon and Bergeron, 1997; Lee *et al.*, 1999). This cluster also seems to be dominated by both medium-molecular weight (MMW = 4-5 rings) and high-molecular weight (HMW = 6 rings) PAHs (Fig. 2D). Note that low-molecular weight (LMW= 2-3 rings) PAHs are minor contributors to both clusters (Fig. 2D). PAH C#2 mostly represents samples retrieved from the Upper Estuary and Gulf of St. Lawrence. PAH C#2 samples also contain a higher proportion of HMW and MMW PAHs (Fig. 2D). The generated principal coordinate ordination diagram (Fig. 2B) and silhouette plot (Fig. S1) confirm the robustness of the above clusters. However, 5 samples retrieved from PAH C#1 and 7 samples retrieved from PAH C#2 attain lower than average (0.15) or negative silhouette values, indicating a questionable assignment (Figs. 2C and S1). Indeed, these samples are located at the boundary between PAH C#1 and PAH C#2, as shown in Fig. 2B, suggesting a mixture of PAH assemblages and sources.

The TOC content in the surface samples (<150 µm fraction) ranges from 0.1 in the coarse-grained sediment samples (sand and silty sand) to 2.3% in the fine-grained sediment samples (sandy silt and silt) (Figs. 3 and 4A, respectively). Both PAH clusters exhibit an

average TOC content of 1.1 ± 0.4%. Higher TOC contents (>1.7%) are found in the Baie-des-Chaleurs inlet area, a biologically highly productive area, offshore Matane near a pockmark, and close to the mouth of the Saint-Charles River in Québec city, an area strongly influenced by anthropic activities.

The sums of the concentrations of the 16 priority PAHs (Σ_{16}PAHs, dry weight or dw) identified by the US EPA in the surface sediments of the EGSL range from 71 to 5672 ng g^{-1} with a mean value of 325 ng g^{-1} (three statistical outliers are not considered; Fig. 4B). Specifically, samples retrieved from PAH C#1 exhibit Σ_{16}PAH concentrations ranging from 265 to 5672 ng g^{-1} with a mean value of 427 ng g^{-1}, while the Σ_{16}PAH concentration in the PAH C#2 samples ranges from 72 ng g^{-1} to 2018 ng g^{-1} with a mean value of 267 ng g^{-1} (Fig. 5A). The highest PAH values are obtained in samples collected near Baie-Comeau (PAH C#1), at 2429 ng g^{-1} (COR2001-02VV, in a harbor area near an aluminum smelter) and 5672 ng g^{-1} (COR2001-06BC, ~ 5 km offshore of the same aluminum smelter harbor). Indeed, the Baie-des-Anglais area, home to an aluminum smelter harbor, a pulp and paper mill, a grain storage facility and a municipal sewage water discharge outlet, contains high concentrations of hydrocarbons and other pollutants in its sediments (Pellerin-Massicotte, 1993; Lee *et al.*, 1999). The area was targeted for long-term monitoring and further pollutant analysis because of the possible risks posed to beluga whales frequenting the area (Multipartite Committee on Contaminated Sites of Concern for the St. Lawrence Beluga, 1998). Moreover, during the 1990s, the PAH content in surface sediments in this area exceeded the PAH toxic effect threshold for beluga whales (Gagnon and Bergeron, 1997). Most obtained values for the surface samples from PAH C#2 fall within the ranges of PAH sum values measured elsewhere along the St. Lawrence River, but they are lower than those in areas under heavy anthropogenic pressure, such as the Saguenay Fjord, Baie-Comeau area and upstream sectors of the St. Lawrence Estuary (e.g., the Great Lakes, Montréal and Québec city) (Table 1). The PAH concentration in estuarine environments near urban centers is generally high given their proximity to watersheds and airsheds (Latimer and Zheng, 2003). Compared to worldwide values (Table 1),the EGSL exhibits PAH levels similar to those in well-urbanized and moderately polluted areas, such as the Pearl River Delta in southern China (Mai *et al.*, 2002). Moreover, the EGSL values are higher than those determined for other rivers with

moderate anthropogenic impacts, such as the San Joaquin River in western USA (Pereira *et al.,* 1996), but lower than those in highly polluted areas, such as Boston Harbor in northeastern USA (Shiaris and Jambard Sweet, 1986). However, given the large differences between published PAH studies (i.e., extraction and quantification methods and number of analyzed PAHs), direct comparisons should be carefully performed.

It has been suggested in several studies that the grain size, sedimentary TOC and black carbon particles (i.e., highly condensed residues and products of incomplete combustion) are important factors influencing the sorption, sequestration, and fate of PAHs in marine sediments (e.g., Oen *et al.,* 2006; Sánchez-García *et al.,* 2010; Gu *et al.,* 2013; Wang *et al.,* 2014; Gu *et al.,* 2016; Ma *et al.,* 2017). In this study, grain size variation (<150 μm fraction) in the EGSL sediments does not influence the PAH concentration in the samples, suggesting that the grain size is a noncritical parameter affecting the regional distribution of PAHs (Fig. 3). Moreover, the nonparametric Spearman rank method was performed to measure the correlation between the TOC and PAH concentrations in each cluster. Note that coarse-grained sediment samples with <0.5% TOC were not included in the above correlation analysis, as these samples are mainly influenced by local coastal processes and therefore considered outliers. A poor correlation is observed between the TOC and PAH concentrations in both PAH clusters (Fig. 5B), which may indicate that sedimentary TOC does not play an important role in the PAH distribution in the EGSL sediments. Poor correlations between the PAHs and TOC concentrations can be obtained when organic pollutant concentrations are strongly influenced by anthropogenic inputs instead of natural inputs (e.g., Mai *et al*., 2002; Gu *et al*., 2013, 2016; Ma *et al.,* 2017). Published data on TOC and PAHs (including Σ_{15}PAHs) based on two sediment cores collected in the Lower Estuary and Gulf of St. Lawrence (Panetta, 2009) also revealed a poor correlation between TOC and PAHs (Fig. 5C), in agreement with our results. However, nonpublished black carbon data (measured in the organic geochemistry environmental laboratory of Y. Gélinas at Concordia University) based on these same sediment cores indicated a significant positive correlation between the soot black carbon and Σ_{15}PAH concentrations (Fig. 5D). Based on these results, we hypothesize that the distribution of PAHs in EGSL sediments is likely controlled by combustion-derived black

carbon particles associated with the intense industrial and marine transport activities occurring in this region.

In regard to the core samples, the approximate age of the basal sediment samples was estimated according to the sedimentation rates reported for collected sediment cores that are similar those obtained in this study (Table 2; Smith and Schafer, 1999). We estimated that the basal sediments of cores AMD18-OSL-03BC, 05BC, 06BC, 07BC and 08BC were most likely deposited prior to 1900 common era or CE (the pre-industrial period), while in terms of cores AMD18-OSL-01BC and 02BC, sediments accumulated after 1900 CE (the post-industrial period). Thus, these sediment core samples provide an opportunity to document the PAH distribution and concentration during the pre- and post-industrial periods.

These core samples exhibit a wide range of the Σ_{16}PAH concentration (Fig. 5A). Indeed, the Σ_{16}PAH concentration in the five pre-industrial samples (1006-1822 CE) ranges from 93 to 172 ng g^{-1} (mean value of 130 ng g^{-1}), which is relatively low and comparable to that in worldwide regions under little to no anthropogenic pressure. For example, the Σ_{16}PAH concentration in sediments retrieved from northern Baffin Bay ranges from 26 – 199 ng g^{-1} (mean value of 106 ng g^{-1}; Foster *et al.*, 2015), and it ranges from 8 to 248 ng g^{-1} in the Canadian Arctic Archipelago (mean value of 57 ng g^{-1}; Corminboeuf *et al.*, 2021). Conversely, the Σ_{16}PAH concentration in the two post-industrial samples (1937-1943 CE) is higher, ranging from 1216 to 1621 ng g^{-1} (mean value of 1419 ng g^{-1}), which is 2.5 times higher on average than the PAH concentration in all surface samples (Fig. 5A). The industrialization process ensuing in North America until the mid-20th century was a source of many pollutants, including PAHs, in the St. Lawrence River (Working Group on the State of the St. Lawrence Monitoring, 2014). It is thus expected that the highest Σ_{16}PAH values occur in sediments deposited during this period (Table 2). In 1988, the St. Lawrence Action Plan targeted 50 priority plants discharging suspended solids, organic matter, oils, greases and metals directly into the St. Lawrence River (Working Group on the State of the St. Lawrence Monitoring, 1994). These plants mainly stemmed from the pulp and paper sector and metallurgy sector. Following the first phase of the St. Lawrence Action Plan, which occurred between 1988 and 1993, a 74% reduction in liquid toxic waste (including PAHs, metals and polychlorinated biphenyls or

PCBs) released into the St. Lawrence River was achieved in 1993. Specifically, the Canadian Reynolds Metal Company at Baie-Comeau (which was later bought by Alcoa and is an actual aluminum smelter) successfully reduced its PAH emissions by 99% (Working Group on the State of the St. Lawrence Monitoring, 1994). This reduction in industrial PAH emissions could explain the lower PAH values determined in the surface sediments retrieved from the EGSL than those in sediment samples deposited in the early 20th century (Fig. 5A).

Because PAHs are emitted as a mixture and since their relative proportions depend on the emission sources, it is possible to determine the origin based on the diagnostic ratios between specific compounds (Tobiszewski and Namieśnik, 2012). The ratios of fluoranthene over the sum of fluoranthene and pyrene (Fla/[Fla+Pyr]) and of benz(a)anthracene over the sum of benz(a)anthracene and chrysene (BaA/[BaA+Chr]) are generally considered for sediments (e.g., Yunker *et al.*, 2002; Foster *et al.*, 2015; Gu *et al.*, 2013, 2016; Ma *et al.*, 2017; Corminboeuf *et al.*, 2021). Fla/[Fla+Pyr] values below 0.4 suggest a petrogenic source, while values between 0.4 and 0.5 are characteristic of fossil fuel combustion, and values above 0.5 indicate a biomass combustion source (Yunker *et al.*, 2002). Generally, BaA/[BaA+Chr] diagnostic ratio values below 0.2 indicate a petrogenic source, while ratio values between 0.2 and 0.35 correspond to mixed sources, and ratio values above 0.35 suggest a pyrogenic source (Yunker *et al.*, 2002). In our dataset, the PAH C#1 samples exhibit Fla/[Fla+Pyr] values ranging from 0.35 to 0.60 with a mean value of 0.46 and BaA/[BaA+Chr] values ranging from 0.25 to 0.45 with a mean value of 0.35 (Fig. 6). These two ratios suggest that both fossil fuel combustion and pyrogenic sources are responsible for the PAHs detected in our samples. The PAH C#1 samples are positively correlated with parent PAHs containing 4 to 6 rings, such as dibenz(a,h)anthracene, benz(a)anthracene, indeno(1,2,3-c,d)pyrene, benzo(g,h,i)perylene, benzo(b)fluoranthene and benzo(a)pyrene (Fig. 7), which are commonly associated with pyrogenic PAHs (Balmer *et al.*, 2019). These results are consistent with anthropogenic signatures in urbanized areas and the deposition of pyrogenic atmospheric PAHs.

The PAH C#2 samples exhibit Fla/[Fla+Pyr] values ranging from 0.05 to 0.56 (mean value of 0.38) and BaA/[BaA+Chr] values ranging from 0.19 to 0.40 (mean value of 0.31) (Fig. 6). Both clusters and ratios indicate a mixed/pyrogenic source for the detected

PAHs. The primary natural atmospheric source of PAHs in Canada is forest fires, while the main anthropogenic atmospheric sources in the province of Québec include residential wood heating and aluminum smelters (Working Group on the State of the St. Lawrence Monitoring, 2014). The main sources of PAHs in water and sediments are spills of petroleum products, various industries (e.g., metal manufacturing and coke plants) and atmospheric deposition (Working Group on the State of the St. Lawrence Monitoring, 2014). Additionally, atmospheric deposition accounts for a major PAH source near urban areas (Laflamme and Hites, 1978; Latimer and Zheng, 2003), which can explain the pyrogenic signature observed in our samples. However, certain samples retrieved from the PAH C#2 cluster also occur within the petrogenetic signature zone (Fig. 6). The PAH C#2 samples are strongly correlated with alkylated PAHs (i.e., 1-methylnaphthalene, 2-methylnaphthalene, 2,6-dimethylnatphthalene and 1-methylphenanthrene; Fig. 7), which are mostly associated with noncombustion-derived petrogenic PAHs (Balmer *et al.,* 2019). The presence of active pockmarks in the Laurentian Channel (Pinet *et al.,* 2008; Lavoie *et al.,* 2010) might explain the observed strong correlation between the PAH C#2 samples and naturally derived alkylated PAHs (e.g., Boitsov *et al.,* 2009). More than 2000 pockmarks with a diameter ranging from a few tens of meters up to 700 m have been identified in the Lower Estuary, with approximately 109 pockmarks located offshore of Matane (Pinet *et al.*, 2010; Lavoie *et al.*, 2010). In the gulf, many pockmarks have also been found along the Laurentian Channel (mainly in the Old Harry sector) and Baie-des-Chaleurs area (Fader, 1991; Lavoie *et al*., 2009), but these pockmarks remain scarcely documented (Sirdeys, 2019). Overall, the PAH C#2 samples are therefore influenced by both petrogenic PAHs stemming from pockmarks and pyrogenic PAHs attributed to atmospheric deposition.

The source-diagnostic PAH ratios determine for the basal sediments in the cores exhibit a clear separation between the pre- and post-industrial samples (Fig. 6). Indeed, the Fla/[Fla+Pyr] values for the pre-industrial samples (1006-1822 CE) range from 0.25 to 0.49 (mean value of 0.41), which indicates a greater petrogenic influence with some fossil combustion contribution (Fig. 6). The only two BaA/[BaA+Chr] values available for the pre-industrial samples are 0.20 and 0.22, which occur on the ratio boundary between petrogenic and pyrogenic sources, in agreement with the Fla/[Fla+Pyr] ratio. Conversely,

the Fla/[Fla+Pyr] values for the two post-industrial samples (1937-1943 CE) are 0.45 and 0.49, suggesting a fossil fuel combustion source (Fig. 6). The BaA/[BaA+Chr] values for these 2 same samples are 0.37 and 0.42, respectively, which suggest a pyrogenic influence consistent with the previous ratios. These results highlight the impact of anthropogenic PAH inputs into the sediments retrieved from the EGSL during the industrialization period. This also enables us to document that the efforts implemented during the 1980s and 1990s targeting toxic liquid discharge reduction (including PAHs) into the St. Lawrence River not only led to a reduction in the PAH content in sediments but also drove the corresponding PAH source signatures slightly more into the petrogenic and natural zones.

The effects range-low (ERL, the probability of adverse biological effects is <10%) and effects range-median (ERM, the probability of adverse biological effects is >50%) are useful and easily accessible guideline values proposed by Long *et al.* (1995) to quickly determine the potential ecological risk of the PAH content in sediments. In most of the sediment samples collected across the EGSL, the PAH content is below both values (Table 3). However, the ERL threshold value is exceeded at certain stations, namely, those stations with acepathene, phenanthrene, benzo(a)pyrene and dibenz(a,h)anthracene concentrations above the ERL are located in the Baie-Comeau area, which is understandable given the known industrial anthropogenic influences, as documented above (Fig. 4B). A station with fluorene and pyrene levels exceeding the corresponding ERL values is located offshore of Matane and is therefore likely influenced by the well-documented active pockmarks in this area (Pinet *et al.*, 2010). Excluding these stations, no results exceed the ERL values (Table 3), indicating that benthic or other organisms living near the water-sediment interface are exposed to a low ecological risk regarding these pollutants.

This study provides a robust spatial distribution inventory of pre- and post-industrial PAH levels in EGSL sediments. Statistical analysis indicates that the Lower Estuary sediments (mainly in the Baie-Comeau-Matane area) exhibit distinct PAH signatures over the Upper Estuary and Gulf sediments. The highest Σ_{16}PAH values in surface sediments were found in the Baie-Comeau area (2429 - 5672 ng g^{-1}), which is consistent with the known anthropogenic pressure stemming from the industrialized sector. The basal sediments in the cores corresponding to the early post-industrial period reveal higher Σ_{16}PAH levels (mean value of 1419 ng g^{-1}) than those in modern sediments (mean

value of 325 ng g^{-1}), while the pre-industrial core samples reveal the lowest values (mean value of 130 ng g^{-1}). Most of the surface sediment samples collected in the EGSL exhibit Σ_{16}PAH concentrations similar to those in other well-urbanized estuarine systems. The PAH concentration and distribution in the EGSL sediments are mainly governed by black carbon particles derived from anthropogenic emissions. Indeed, the source-diagnostic PAH ratios suggest that (1) pyrogenic PAHs originating from atmospheric deposition dominate, with a minor influence of petrogenic sources derived from seabed pockmarks, and (2) pyrogenic sources constitute the primary sources of PAHs in Lower Estuary sediments deposited during the early postindustrial period. Finally, most of the sediment samples obtained from the EGSL contain PAH contents below the ERL value, which indicates a low ecological risk to benthic or other organisms living near the water-sediment interface. Overall, the baseline data provided here are of great value for resource management of the marine areas in the EGSL.

Acknowledgments

We acknowledge the captains, officers, crews, and scientific participants of AMD18-OSL, AMD19-OSL, and AMD20-OSL onboard CCGS Amundsen and the 2020 RQM-MEOPAR expedition onboard R/V Coriolis II for the recovery of the sediment samples analyzed in this study. We thank Marie-Pier St-Onge (RQM), Claude Belzile (ISMER-UQAR), Dominique Lavallée (ISMER-UQAR), Steeven Ouellet (UQAR), Agnieszka Adamowicz (Geotop), and Jean-François Hélie (Geotop) for the provided technical support at sea and in the laboratory. Part of this research was supported by the RQM through the Odyssée Saint-Laurent research program, by the Natural Sciences and Engineering Research Council of Canada (NSERC) through Discovery Grants provided to J.-C. Montero-Serrano, and by Québec-Océan, Geotop and Amundsen Science. All analytical data presented are available electronically in the St. Lawrence Global Observatory database (https://ogsl.ca/en/home-slgo/).

Appendix A. Supplementary data

Supplementary data for this article can be found online at http: XXX.

CRediT authorship contribution statement
Anne Corminboeuf: investigation, writing – original draft.
Allyson Dalpé: Sample preparation, investigation.
Jean-Carlos Montero-Serrano: conceptualization, resources, writing – review and editing, funding acquisition.
Richard St-Louis: resources, writing – review and editing.
Yves Gélinas: investigation, writing – review and editing

Declaration of competing interest

All authors declare that there are no conflicts of interest regarding the publication of this paper. The first two authors contributed equally to this paper.

References

Aitchison, J.1986. The statistical analysis of compositional data. Monographs on statistics and applied Probability: Chapman & Hall, London (Reprinted in 2003 with additional material by Blackburn Press), 416 p.

Aitchison, J. 1990. Relative variation diagrams for describing patterns of compositional variability. Mathematical Geology, 22(4), 487–511.

AMAP, 2017. AMAP Assessment 2016: Chemical of emerging Arctic concern. Arctic Monitoring and Assessment Program (AMAP), Oslo, Norway, (16) 353.

Barletta, F., St-Onge, G., Stoner, J.S., Lajeunesse, P., Locat, J. 2010. A high-resolution Holocene paleomagnetic secular variation and relative paleointensity stack from eastern Canada. Earth and Planetary Science Letters, 298(1), 162–174.

Balmer, J.E., Hung, H., Yu, Y., Letcher, R.J., Muir, D.C.G. 2019. Sources and environmental fate of pyrogenic polycyclic aromatic hydrocarbons (PAHs) in the Arctic. Emerging Contaminants, 5, 128-142.

Boitsov, S., Jensen, H.K.B., Klungsøyr, J. 2009. Natural background and anthropogenic inputs of polycyclic aromatic hydrocarbons (PAH) in sediments of the south-western Barents Sea. Marine Environmental Research, 68, 236-245.

Borcard, D., Gillet, F., Legendre, P. 2011. Numerical ecology with R, Springer, New York.

Buell, M.-C., Johannessen, C., Drouillard, K., Metcalfe, C. 2021, in press. Concentrations and source identification of PAHs, alkyl-PAHs and other organic contaminants in sediments from a contaminated harbor in the Laurentian Great Lakes (https://doi.org/10.1016/j.envpol.2020.116058)

Camu, P., Benedict, R.W., Hamelin, L.-E. 2019. St. Lawrence River and Seaway, Encyclopædia Britannica, [online], URL: https://www.britannica.com/place/Saint-Lawrence-River

Charrad, M., Ghazzali, N., Boiteau, V., Niknafs, A. 2014. Nbclust: an R package for determining the relevant number of clusters in a data set. Journal of Statistical Software, 61, 1–36.

Chen, F., Lin, Y., Cai, M., Zhang, J., Zhang, Y., Kuang, W., Liu, L., Huang, P., Ke, H. 2018. Occurrence and risk assessment of PAHs in surface sediments from Western Arctic and Subarctic Ocean. International Journal of Environmental Research and Public Health, 15, 734.

Choi, M., Kim., Y.-J., Lee, I.-S., Choi, H.-G. 2014. Development of a one-step integrated pressurized liquid extraction and cleanup method for determining polycyclic aromatic hydrocarbons in marine sediments. Journal of Chromatography A, 1340, 8-14.

Corminboeuf, A., Montero-Serrano, J.-C., St-Louis, R. 2021. Spatial and Temporal Distributions of Polycyclic Aromatic Hydrocarbons in Sediments from the Canadian Arctic Archipelago. ChemRxiv. Preprint. https://doi.org/10.26434/chemrxiv.14055398.v1

El-Sabh, M.I., Silverberg, N. 1990. Oceanography of a Large-Scale Estuarine System; The St. Lawrence, Spring-Verlag, New-York.

Fader, G.B. J. 1991. Gas-related sedimentary features from the eastern Canadian continental shelf. Continental Shelf Research, 11(8-10), 1123-1153.

Foster, K.L., Stern, G.A., Carrie, J., Bailey, J.N.-L., Outridge, P.M., Sanei, H., Macdonald, R.W. 2015. Spatial, temporal, and source variations of hydrocarbons in marine sediments from Baffin Bay, Eastern Canadian Arctic. Science of the Total Environment, 506-507, 430-443.

Gamboa, A., Montero-Serrano, J.-C., St-Onge, G., Rochon, A., Desiage, P. 2017. Mineralogical, geochemical and magnetic signatures of surface sediments fromthe Canadian Beaufort Shelf and Amundsen Gulf (Canadian Arctic). Geochemistry, Geophysics, Geosystems 25, 488–512.

Gagnon, M., Bergeron, P. 1997. Identification et description des sites aquatiques contenant des contaminants préoccupants pour le béluga du Saint-Laurent. Rapport de Biorex inc. au Comité multipartite sur les sites contaminés pouvant affecter le béluga. 180 p

Gearing, J. N., P. J. Gearing, M. Noël et J. N. Smith. 1994. Polycyclic aromatic hydrocarbons in sediment of the St. Lawrence estuary. Dans: *Proceedings of the Twentieth Annual Aquatic Toxicity Workshop, October 17-21, 1993, Québec*. R. Coillie, Y. Roy, Y. Bois, P. G. C. Campbell, P. Lundahl, L. Martel, M. Michaud, P.

Riebel et C. Thellan (eds.). Rapport Technique Canadien sur les pêcheries et les sciences aquatiques 1989. p.58-64.

Genovesi, L., de Vernal, A., Thibodeau, B., Hillaire-Marcel, C., Mucci, A., 2011. Recent changes in bottom water oxygenation and temperature in the Gulf of St. Lawrence: micropaleontological and geochemical evidence. Limnology and Oceanography, 56, 1319–1329.

Government of Canada. 1994. Polycyclic aromatic hydrocarbons, Canadian Environmental Protection Act: Priority substances list assessment report. [PDF], URL: https://www.canada.ca/content/dam/hc-sc/migration/hc-sc/ewh-semt/alt_formats/hecs-sesc/pdf/pubs/contaminants/psl1-lsp1/hydrocarb_aromat_polycycl/hydrocarbons-hydrocarbures-eng.pdf

Government of Canada. 2017. St. Lawrence River: overview, [online], URL: https://www.canada.ca/fr/environnement-changement-climatique/services/fleuve-saint-laurent.html

Gu, Y.G., Lin, Q., Lu, T.T., Ke, C.L., Sun, R.X., Du, F.Y. 2013. Levels, composition profiles and sources of polycyclic aromatic hydrocarbons in surface sediments from Nan'ao Island, a representative mariculture base in South China. Marine Pollution Bulletin, 75, 310–316.

Gu, Y.G., Ke, C.L., Liu, Q., Lin, Q., 2016. Polycyclic aromatic hydrocarbons (PAHs) in sediments of Zhelin Bay, the largest mariculture base on the eastern Guangdong coast, South China: Characterization and risk implications. Marine Pollution Bulletin 110, 603–608.

Haritash, A.K., Kaushik, C.P. 2009. Biodegradation aspects of polycyclic aromatic hydrocarbons (PAHs): A review. Journal of Hazardous Materials, 169, 1-15.

Hélie, J.-F. 2009. Elemental and stable isotopic approaches for studying the organic and inorganic carbon components in natural samples. IOP Conference Series: Earth Environmental Science, 5, 012005.

Kassambara, A., Mundt, F. 2020. Factoextra: Extract and Visualize the Results of Multivariate Data Analyses. R Package Version 1.0.7. [Available at https://cran.r-project.org/web/packages/factoextra/]

Kaufman, L., Rousseeuw, P.J. 2009. Finding groups in data: an introduction to cluster analysis, John Wiley & Sons.

Keith, L.H. 2014. The Source of U.S. EPA's sixteen PAH priority pollutants. Polycyclic Aromatic Compounds, 35, 147-160.

Klungsøyr, S.L., Dahle, S., Thomas, D.J. 2010. Sources, inputs and concentrations of petroleum hydrocarbons, polycyclic aromatic hydrocarbons, and other contaminants related to oil and gas activities in the Arctic. In: AMAP Assessment 2007: Oil and gas activities in the Arctic – Effects and Potentiel Effects. Volume 2, chapter 4. Arctic Monitoring and Assessment Programme (AMAP).

Laflamme, R.E., Hites, R.A. 1978. The global distribution of polycyclic aromatic hydrocarbons in recent sediments. Geochimica et Cosmochimica Acta, 41, 289-303.

Latimer, J.S., Zheng, J. 2003. Sources, Transport, and Fate of PAHs in the Marine Environment. In PAHs: An Ecotoxicological perspective, Douben, P.E.T. (Ed.), John Wiley & Sons.

Lavoie, D., Pinet, N., Dietrich, J., Hannigan, P., Castonguay, S., Hamblin, A.P., Giles, P. 2009. Petroleum Resource Assessment, Paleozoic successions of the St. Lawrence Platform and Appalachians of eastern Canada. Geological Survey of Canada, Open File 6174.

Lavoie, D., Pinet, N., Duchesne, M., Bolduc, A., Larocque, R. 2010. Methane-derived authigenic carbonates from active hydrocarbon seeps of the St. Lawrence Estuary, Canada. Marine and Petroleum Geology, 27, 1262-1272.

Lee, K., Nagler, J.J., Fournier, M., Lebeuf, M., Cyr, D.G. 1999. Toxical characterization of sediments from Baie des Anglais on the St. Lawrence Estuary. Chemosphere, 39(6), 1019-1035.

Lima, A.L., Farrington, J.W., Reddy, C.M. 2005. Combustion-derived polycyclic aromatic hydrocarbons in the environment – A review. Environmental Forensics, 6, 109-131.

Long, E.R., MacDonal, D.D., Smith, S.L., Calder, F.D. 1995. Incidence of adverse biological effects within ranges of chemical concentrations in marine and estuarine sediments. Environmental Management, 19(1), 81-97.

Loring, D.H., Nota, D.J.G. 1973. Morphology and Sediments of the Gulf of St. Lawrence. Bulletin of the Fisheries Research Board of Canada; Environment Canada, Fisheries and Marine Service. Bulletin 182, Ottawa 1973, scale 1:1,000,000

Ma, Y., Halsall, C.J., Xie, Z., Koetke, D., Mi, W., Ebinghaus, R., Gao, G. 2017. Polycyclic aromatic hydrocarbons in ocean sediments from the North Pacific to the Arctic Ocean. Environmental Pollution, 227, 498-504.

Mai, B.-X., Fu, J.-M., Sheng, G.-Y., Kang, Y.-H., Lin, Z., Zhang, G., Min, Y.-S., Zeng, E.Y. 2002. Chlorinated and polycyclic aromatic hydrocarbons in riverine and estuarine sediments from Pearl River Delta, China. Environmental Pollution, 117, 457-474.

Martin Associates. 2018. Economic impacts of maritime shipping in the Great Lakes – St. Lawrence region; Executive summary. [PDF] https://greatlakes-seaway.com/wp-content/uploads/2019/10/eco_impact_sum.pdf

Meek, M.E., Chan, P.K.L., Bartlett, S. 1994. Polycyclic aromatic hydrocarbons evaluation of risks to health from environmental exposure in Canada. Journal of Environmental Science Health, Part C: Environmental Carcinogenesis and Ecotoxicological Reviews, 12(2), 443-452.

Morillo, E., Romero, A.S., Madrid, L., Villaverde, J., Maqueda, C. 2008. Characterization and sources of PAHs and potentially toxic metals in urban environments of Sevilla (Southern Spain). Water, Air and Soil Pollution, 187, 41–51.

Montero-Serrano, J. C., Palarea-Albaladejo, J., Martin-Fernandez, J.-A., Martinez-Santana, M., Gutierrez-Martin, J. V. 2010. Sedimentary chemofacies characterization by means of multivariate analysis. Sedimentary Geology, 228, 218–228, doi:10.1016/j.sedgeo.2010.04.013.

Montero-Serrano, J.-C., Rioux, P., Boutot, C., Letaeif S. 2018. Dynamique sédimentaire et conditions de surface de l'estuaire et le golfe du Saint-Laurent. Odyssée Saint-Laurent 2018, Rapport de mission, NGCC Amundsen (08 au 24 Février 2018), 11 p.

Montero-Serrano, J.-C., Beauvais, Q., Dhifallah, F., Fabris, A.-S., Rioux, P., Boutot, C. 2019. Dynamique sédimentaire et distribution des kystes de dinoflagellés toxiques dans l'estuaire et le golfe du Saint-Laurent à l'hiver. Odyssée Saint-Laurent 2019, Rapport de mission, NGCC Amundsen (01 au 16 Février 2019), 12 p.

Montero-Serrano, J.-C., Fabris, A.-S., Corminboeuf, A. 2020a. Dynamique sédimentaire et conditions de surface de l'estuaire du Saint-Laurent : échantillonnage de glace de mer, de matériel particulaire en suspension et de sédiments du fond marin. Odyssée Saint-Laurent 2020, Rapport de mission, NGCC Amundsen (27 février au 14 mars 2020), 14 p.

Montero-Serrano J.-C., Limoges A., Normandeau A., Corminboeuf A., Laphengphratheng T. 2020b. R/V Coriolis II expedition RQM-MEOPAR – COR2001: Monitoring natural hazards during coastal to offshore sediment remobilization and its impacts on primary production dynamics in the Lower St. Lawrence Estuary. COR2001 expedition report. Université du Québec à Rimouski (UQAR), Institut des sciences de la mer de Rimouski (ISMER), 54 p. http://semaphore.uqar.ca/id/eprint/1731.

Multipartite Committee on Contaminated Sites of Concern for the St. Lawrence Beluga. 1998. Contaminated Sites of Concern for the St. Lawrence Beluga. Report Presented to the St. Lawrence Vision 2000 Action Plan Management Committee. Environment Canada, Fisheries and Oceans Canada, Canadian Heritage and the Ministère de l'Environnement et de la Faune du Québec. 26 p.

Muzuka, A.N.N., Hillaire-Marcel, C. 1999. Burial rates of organic matter along the eastern Canadian margin and stable isotope constraints on its origin and diagenetic evolution. Marine Geology, 160, 251–270.

Normandeau, A., Lajeunesse, P., St-Onge, G. 2015. Submarine canyons and channels in the Lower St. Lawrence Estuary (Eastern Canada): Morphology, classification and recent sediment dynamics. Geomorphology, 241 (1-18).

Oblinger Childress, C.J., Foreman, W.T., Connor, B.F., Maloney, T.J. 1999. New reporting procedures based on long-term method detection levels and some considerations for interpretation of water-quality data provided by the U.S. Geological Survey National Water Quality Laboratory. US Geological Survey, open-file report 99-193.

Oen, A.M.P., Cornelissen, G., Breedveld, G.D., 2006. Relation between PAH and black carbon contents in size fractions of Norwegian harbor sediments. Environmental Pollution, 141, 370–380.

Page, D.S., Boehm, P.D., Douglas, G.S., Bence, A.E., Burns,W.A., Mankiewicz, P.J. 1999. Pyrogenic polycyclic aromatic hydrocarbons in sediments Record Past human activity: a case study in Prince William Sound, Alaska. Marine Pollution Bulletin, 38, 247-260.

Palarea-Albaladejo J., Martin-Fernandez J.A. 2015. zCompositions — R package for multivariate imputation of left-censored data under a compositional approach. Chemometrics and Intelligence Laboratory Systems 143, 85-96.

Pampanin, D.M., Sydnes, M.O. 2017. Petrogenic polycyclic aromatic hydrocarbons in the aquatic environment: analysis, synthesis, toxicity and environmental impact**.** DOI:10.2174/97816810842751170101

Panetta, R. J., 2009. Molecular and isotopic characterization of organic matter in the St. Lawrence Estuary. PhD thesis. Montreal, Québec. Concordia University, 193 p. https://concordiauniversity.on.worldcat.org/search?queryString=ot:(Spectrum)+976511

Pellerin-Massicotte, J., Vincent, B., Pelletier, É. 1993. Évaluation toxicologique de la baie des Anglais à Baie-Comeau (Québec). Water Pollution Research Journal of Canada, 28(4), 665-686.

Pelletier, E., Desbiens, I., Sargian, P., Côté, N., Curtosi, A., St-Louis, R. 2009. Présence des hydrocarbures aromatiques polycycliques (HAP) dans les compartiments biotiques et abiotiques de la rivière et du fjord du Saguenay. Revue des sciences de l'eau, 22(2), 235-251.

Pereira, W.E., Domagalski, J.L., Hostettler, F.D., Brown, L.R., Rapp, J.B. 1996. Occurrence and accumulation of pesticides and organic contaminants in river sediment, water and clam tissues from the San Joaquin river and tributaries, California. Environmental Toxicology and Chemistry 15 (2), 172–180.

Pinet, N., Duchesne, M. Lavoie D., Bolduc, A., Long, B. 2008. Surface and subsurface signatures of gas seepage in the St. Lawrence Estuary (Canada): Significance to hydrocarbon exploration, Marine and Petroleum Geology, 25, 271-288.

Pinet, N., Duchesne, M. and Lavoie, D. 2010 Linking a linear pockmark train with a buried Palaezoic structure: a case study from the St. Lawrence Estuary. Geo-Marine Letters, 30, 517-522.

R Core Team. 2021. R: A language and environment for statistical computing. R Foundation for Statistical Computing, Vienna, Austria. [Available at https://www.R-project.org/]

Roslund, M.I., Grönroos, M., Rantalainen, A.-L., Jumpponen, A., Romantschuk, M., Parajuli, A., Hyöty, H., Laitinen, O., Sinkkonen, A. 2018. Half-lives of PAHs and temporal microbiota changes in commonly used urban landscaping materials. PeerJ DOI 10.7717/peerj.4508

Sánchez-García, L., Cato, I., Gustafsson, Ö., 2010. Evaluation of the influence of black carbon on the distribution of PAHs in sediments from along the entire Swedish continental shelf. Marine Chemistry, 119, 44–51.

Sirdeys, N. (2019). Pockmarks dans le chenal Laurentien, zone d'Old Harry, golfe du Saint-Laurent (est du Canada). Mémoire. Rimouski, Québec, Université du Québec à Rimouski, Institut des sciences de la mer de Rimouski (ISMER), 101 p. http://semaphore.uqar.ca/id/eprint/1666.

Shepard, F.P. 1954. Nomenclature based on sand-silt-clay ratios. Journal of Sedimentary Petrology, 24, 151–158.

Shiaris, M.P., Jambard-Sweet, D. 1986. Polycyclic aromatic hydrocarbons in surficial sediments of Boston Harbour, Massachusetts, USA. Marine Pollution Bulletin, 17(10), 469-472.

Smith, J.N., Schafer, C.T. 1999. Sedimentation, bioturbation, and Hg uptake in the sediments of the estuary and Gulf of St. Lawrence. Limnology and Oceanography, 44(1), 207-219.

Schlitzer, R. (2021). Ocean Data View, version 5.4.0. [Available at https://odv.awi.de]

St. Lawrence Seaway Corporation Management. 2019. The St. Lawrence Seaway traffic report; 2019 navigation season. [online], URL: https://greatlakes-seaway.com/wp-content/uploads/2020/03/traffic_report_2019_en.pdf

St-Onge, G., Stoner, J.S., Hillaire-Marcel, C. 2003. Holocene paleomagnetic records from the St. Lawrence estuary, eastern Canada: centennial- to millennial-scale geomagnetic

modulation of cosmogenic isotopes. Earth and Planetary Science Letters, 209 (1–2), 113–130.

Tobiszewski, M., Namieśnik, J. 2012. PAH diagnostic ratio for the identification of pollution emission sources. Environmental Pollution, 162, 110-119.

Thibodeau, B., de Vernal, A., Limoges, A. 2013. Low oxygen events in the Laurentian Channel during the Holocene. Marine Geology, 346, 183–191.

Van den Boogaart, K. G., Tolosana-Delgado, R. 2008. "Compositions": a unified R package to analyze compositional data. Computers & Geosciences, 34(4), 320-338.

Van Schooten, F.J. 1991. Polycyclic aromatic hydrocarbon - DNA adducts in mice and humans. Academic thesis, State University of Leiden, The Netherlands.

von Eynatten, H., Barceló-Vidal, C., Pawlowsky-Glahn, V. 2003. Sandstone composition and discrimination: A statistical evaluation of different analytical methods: Journal of Sedimentary Research, 73(1), 47-57.

Wang, Z., Liu, Z., Xu, K., Mayer, L. M., Zhang, Z., Kolker, A. S., Wu, W. (2014). Concentrations and sources of polycyclic aromatic hydrocarbons in surface coastal sediments of the northern Gulf of Mexico. Geochem Trans 15, 2. https://doi.org/10.1186/1467-4866-15-2

Working Group on the State of the St. Lawrence Monitoring, 1994. Summary Report 1988-1993. St. Lawrence Action Plan. Environment Canada, Québec's ministère du Développement durable, de l'Environnement et de la Lutte contre les changements climatiques, Québec's ministère des Forêts, de la Faune et des Parcs, Parks Canada, Fisheries and Oceans Canada, and Stratégies Saint-Laurent. 49 p. [Available at: http://planstlaurent.qc.ca/fileadmin/publications/rap_quin_89_93/Five_year_report_1988_1993.pdf]

Working Group on the State of the St. Lawrence Monitoring, 2014. Overview of the State of the St. Lawrence 2014. St. Lawrence Action Plan. Environment Canada, Québec's ministère du Développement durable, de l'Environnement et de la Lutte contre les changements climatiques, Québec's ministère des Forêts, de la Faune et des Parcs, Parks Canada, Fisheries and Oceans Canada, and Stratégies Saint-Laurent. 52 p. [Available at: https://www.planstlaurent.qc.ca/fileadmin/publications/portrait/Portrait_global_2014_150_ANG.pdf]

Xue, W., D. Warshawsky. 2005. Metabolic activation of polycyclic and heterocyclic aromatic hydrocarbons and DNA damage: a review. Toxicology and Applied Pharmacology, 206:73-93.

Yanik, P.J., O'Donnell, T.H., Macko, S.A., Qian, Y., Kennicutt II, M.C. 2003.The isotopic compositions of selected crude oil PAHs during biodegradation. Organic Geochemistry, 34, 291–304.

Yu, Y., Katsoyiannis, A., Bohlin-Nizzetto, P., Brorström-Lundén, E., Ma, J., Zhao, Y., Wu, Z., Tych, W., Mindham, D., Sverko, E., Barresi, E., Dryfhout-Clark, H., Fellin, P., Hung, H. 2019. Polycyclic aromatic hydrocarbons not declining in Arctic air despite global emission reduction. Environmental Science & Technology, 53, 2375-2382.

Yunker, M.B., Macdonald, R.W., Vingarzan, R., Mitchell, R.H., Goyette, D., Sylvestre, S. 2002. PAHs in the Fraser River basin: a critical appraisal of PAH ratios as indicators of PAH source and composition. Organic Geochemistry, 33, 489-515.

Figure captions

Fig. 1. Locations of the sediment samples collected in the Estuary and Gulf of St. Lawrence (EGSL) in eastern Canada. The white labels and dashed lines indicate EGSL subdivisions, while the black squares indicate the selected cities. The orange pentagons indicate the location of the two sediment cores collected by Panetta (2009) and discussed in this study. Abbreviations: BC = box core; VV = Van Veen grab sampler; SF = Saguenay Fjord; PdM = Pointe-des-Monts; BdC = Baie-des-Chaleurs; MS = Magdalen Shallows; LC = Laurentian Channel; AC = Anticosti Channel.

Fig. 2. (A) Optimal number of PAH clusters based on the average silhouette method; (B) ordination of the fuzzy clusters (principal coordinate analysis, PCoA). In this figure, each cluster is associated with a small pie chart whose segment radii are proportional to its membership coefficient; (C) map illustration of the FCM clustering results for the surface samples; (D) ternary diagram for the surface samples showing the relative contributions of the low-molecular weight (LMW, 2-3 rings), medium-molecular weight (MMW, 4-5 rings) and high-molecular weight (HMW, 6 rings) parent PAHs.

Fig. 3. Ternary diagram showing Shepard's sediment classification (Shepard, 1954) of the <150 µm fraction in the EGSL surface sediments.

Fig. 4. Spatial distributions of the (A) TOC (%) content and (B) Σ_{16}PAHs (ng g^{-1}, dw) in the EGSL surface sediments. The red rectangles indicating the stations in (B) correspond to the basal samples from the sediment cores studied here.

Fig. 5. (A) Box plots for Σ_{16}PAHs separated by the clusters and pre- and post-industrial sediment samples. (B-C) Correlation of TOC versus the PAH concentration for each PAH cluster and for the two sediment cores collected in the Lower Estuary (core 23) and Gulf (core 20). Note that in (B), the three outlier samples (AMD18-OSL-03BC, COR2001-06BC, and COR2001-02VV) with the highest sums of PAHs (>1500 ng g^{-1}, dw) are excluded from the correlation analysis. (D) Correlation between the soot organic carbon (OC) (black carbon) and Σ_{15}PAH concentrations in the two identical sediment cores in (C). The TOC and PAH data pertaining to cores 23 and 20 are obtained from Panetta (2009), while the soot OC data for these same cores are nonpublished data stemming from the organic geochemistry environmental laboratory of Y. Gélinas at Concordia University.

Fig. 6. (A) Ratios of fluoranthene over the sum of fluoranthene and pyrene (Fla/[Fla+Pyr]) and (B) ratios of benz(a)anthracene over the sum of benz(a)anthracene and chrysene (BaA/[BaA+Chr]) for all EGSL sediment samples.

Fig. 7. Biplot of principal component analysis (PCA) based on centered log-ratio PAH data for the EGSL surface samples. The color scale gradient on the right indicates the contribution percentage of each PAH to the overall variance in the data. The center of each cluster is plotted as a larger circle.

Table captions

Table 1. Comparison of the ΣPAH values in EGSL marine sediments, as well as those in the sediments of other regions of the St. Lawrence River hydrological basin and worldwide river and estuarine sediments. SLE = St. Lawrence Estuary. [a] The mean value, if available, is reported in parentheses. * Only the median value is available.

Table 2. Estimated age (common era, CE) of the basal core samples based on the sedimentation rates estimated by Smith and Schafer (1999) for nearby sediment cores, as well as their Σ_{16}PAH concentrations. The bold dates indicate the post-industrial samples.

Table 3. Risk assessment of the PAHs in the sediments retrieved from the study area. The red values indicate detected PAH levels that are higher than the ERL values. *The ERL and ERM values are obtained from Long *et al.* (1995).

Supplementary material

Fig. S1. Silhouette plot of fuzzy clustering of the surface samples retrieved from the EGSL based on the PAH concentration. This plot allows visualization of the robustness of clusters, where lower than average negative or negative silhouette values indicate an incorrect and/or questionable assignment. The plot indicates that most of the surface samples are correctly classified.

Table S1. Results of procedural blanks from the PAH analysis. * < MDL = Not detected.

Table S2. Method detection limit (MDL) calculated from the 7 replicates.

Table S3. Content range (ng g^{-1}, dw) for each PAH detected in this study. The mean value is reported in parentheses.

Table S4. Coordinates, water depths, cluster, grain size (<150 μm fraction), TOC, and PAH data for the studied surface sediment samples.

Figure 1

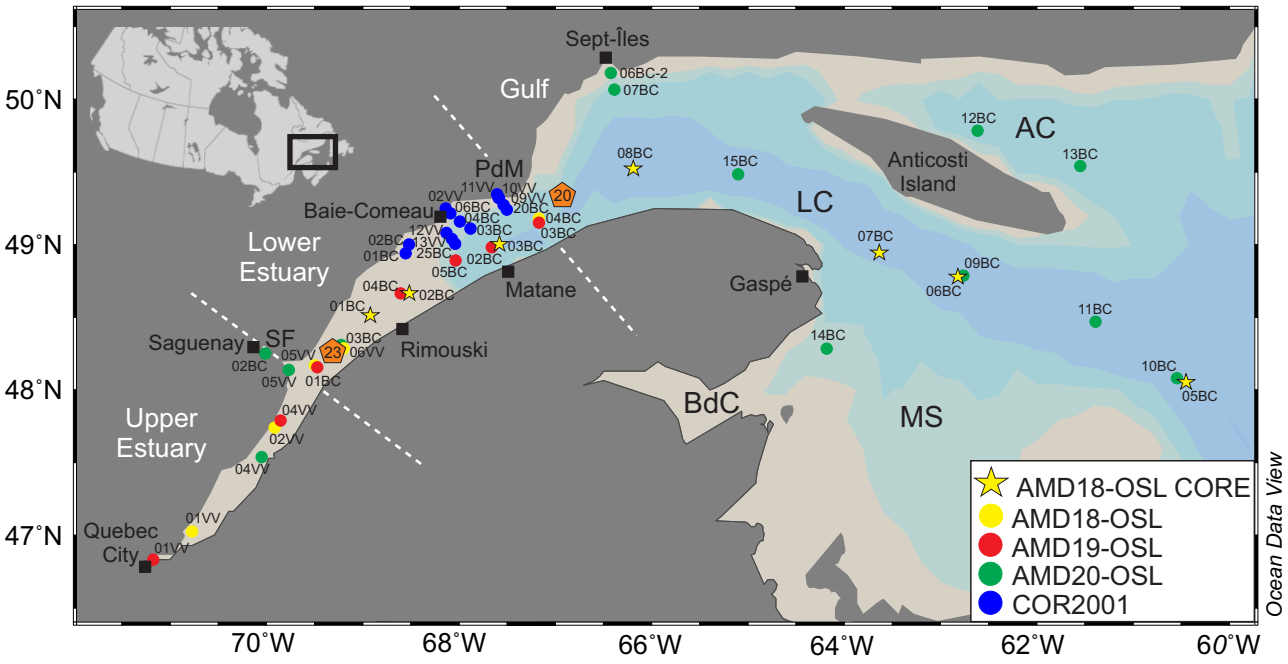
Sept-Îles
Gulf
06BC-2
07BC
12BC
AC
13BC
08BC
15BC
Anticosti
Island
PdM
LC
Baie-Comeau
Lower
Estuary
07BC
09BC
06BC
Gaspé
Matane
11BC
14BC
Saguenay
SF
Rimouski
10BC
05BC
BdC
MS
Upper
Estuary
Quebec
City
AMD18-OSL CORE
AMD18-OSL
AMD19-OSL
AMD20-OSL
COR2001
50˚N
49˚N
48˚N
47˚N
70˚W
68˚W
66˚W
64˚W
62˚W
60˚W
Ocean Data View

Figure 2

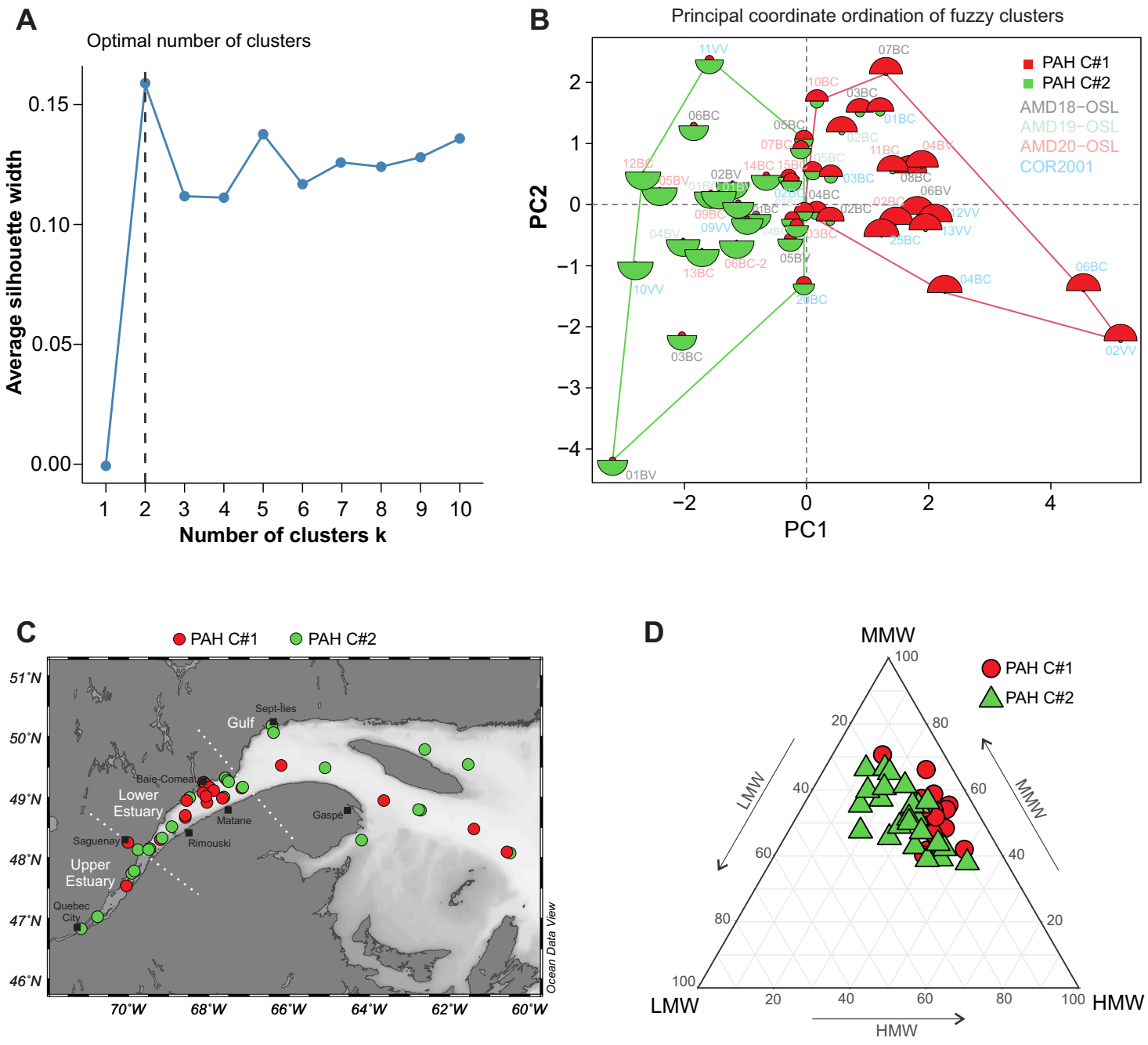
A
Optimal number of clusters
Average silhouette width
0.00
0.05
0.10
0.15
1 2 3 4 5 6 7 8 9 10
Number of clusters k
B
Principal coordinate ordination of fuzzy clusters
PAH C#1
PAH C#2
AMD18−OSL
AMD19−OSL
AMD20−OSL
COR2001
PC2
PC1
C
PAH C#1
PAH C#2
Sept-Îles
Gulf
Baie-Comeau
Lower Estuary
Matane
Gaspé
Saguenay
Rimouski
Upper Estuary
Quebec City
51°N
50°N
49°N
48°N
47°N
46°N
70°W
68°W
66°W
64°W
62°W
60°W
Ocean Data View
D
MMW
PAH C#1
PAH C#2
LMW
HMW

Figure 3

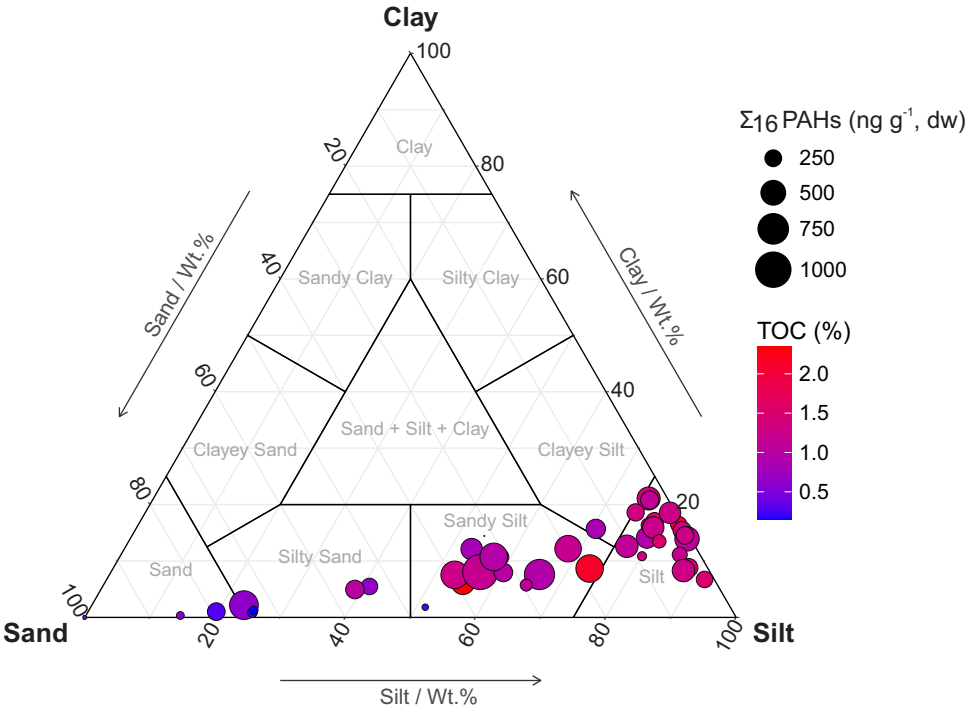
Clay
Sand
Silt
100
80
60
40
20
Clay
Sandy Clay
Silty Clay
Clayey Sand
Sand + Silt + Clay
Clayey Silt
Sandy Silt
Silty Sand
Sand
Silt
Sand / Wt.%
Clay / Wt.%
Silt / Wt.%
Σ16 PAHs (ng g-1, dw)
250
500
750
1000
TOC (%)
2.0
1.5
1.0
0.5

Figure 4

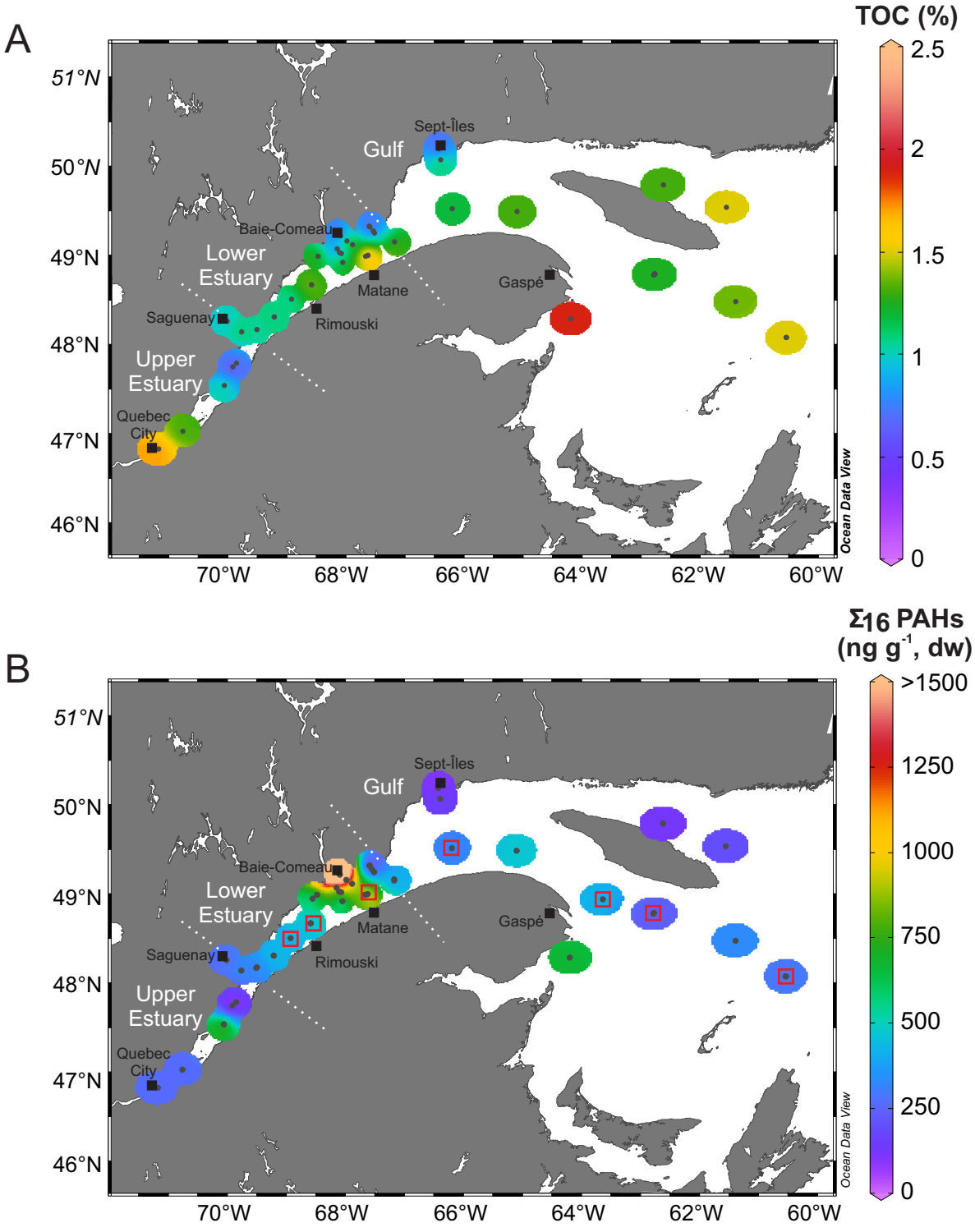
A
TOC (%)
2.5
2
1.5
1
0.5
0
51°N
50°N
49°N
48°N
47°N
46°N
70°W
68°W
66°W
64°W
62°W
60°W
Gulf
Sept-Îles
Baie-Comeau
Lower Estuary
Matane
Gaspé
Saguenay
Rimouski
Upper Estuary
Quebec City
Ocean Data View
B
Σ16 PAHs (ng g-1, dw)
>1500
1250
1000
750
500
250
0
51°N
50°N
49°N
48°N
47°N
46°N
70°W
68°W
66°W
64°W
62°W
60°W
Gulf
Sept-Îles
Baie-Comeau
Lower Estuary
Matane
Gaspé
Saguenay
Rimouski
Upper Estuary
Quebec City
Ocean Data View

Figure 5

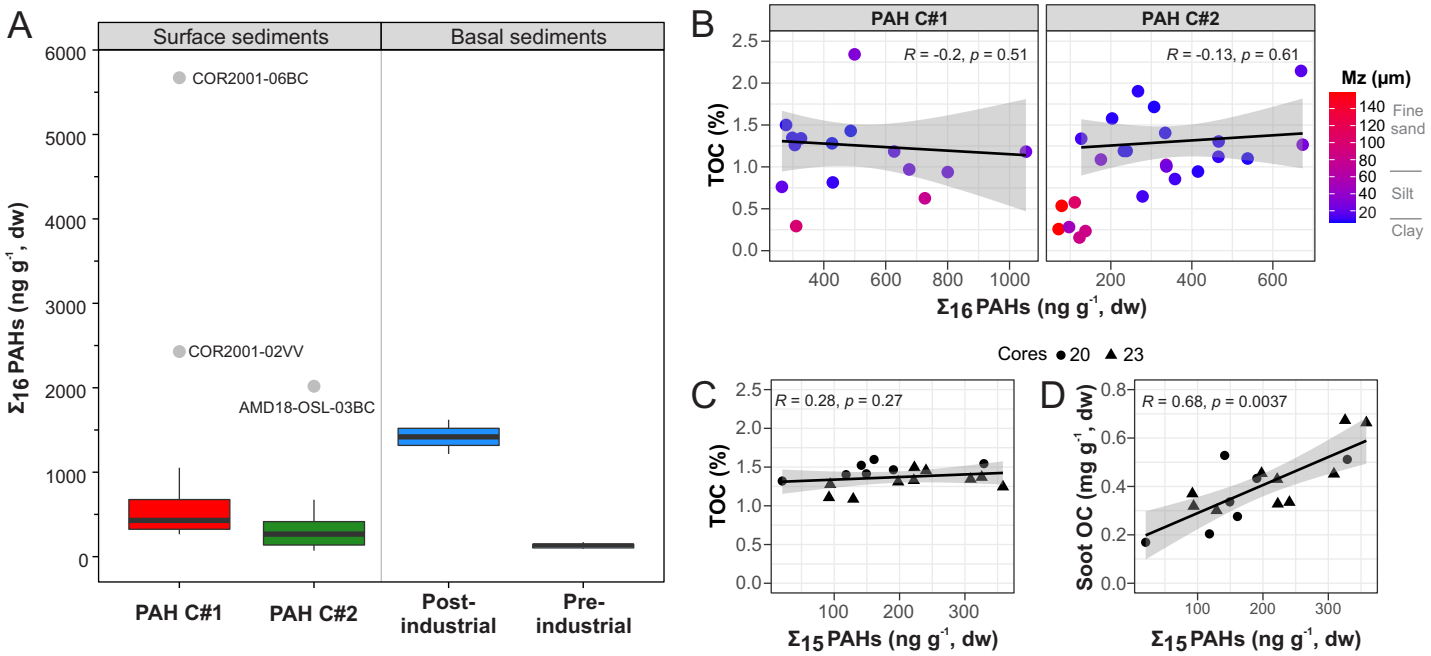
A
Surface sediments
Basal sediments
COR2001-06BC
COR2001-02VV
AMD18-OSL-03BC
Σ16 PAHs (ng g-1, dw)
PAH C#1
PAH C#2
Post-industrial
Pre-industrial
B
PAH C#1
PAH C#2
R = -0.2, p = 0.51
R = -0.13, p = 0.61
TOC (%)
Σ16 PAHs (ng g-1, dw)
Mz (μm)
Fine sand
Silt
Clay
Cores ● 20 ▲ 23
C
R = 0.28, p = 0.27
TOC (%)
Σ15 PAHs (ng g-1, dw)
D
R = 0.68, p = 0.0037
Soot OC (mg g-1, dw)
Σ15 PAHs (ng g-1, dw)

Figure 6

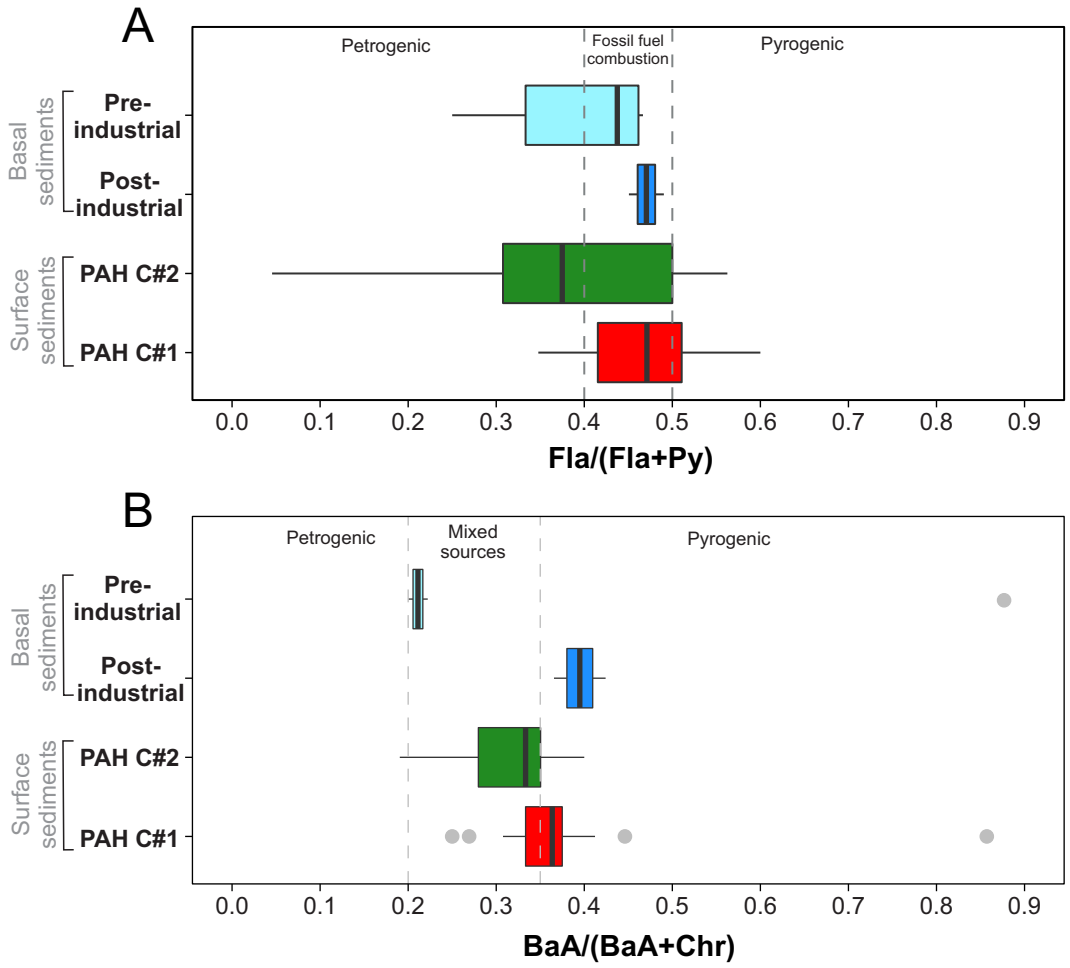
A
Petrogenic
Fossil fuel combustion
Pyrogenic
Basal sediments
Pre-industrial
Post-industrial
Surface sediments
PAH C#2
PAH C#1
0.0
0.1
0.2
0.3
0.4
0.5
0.6
0.7
0.8
0.9
Fla/(Fla+Py)
B
Petrogenic
Mixed sources
Pyrogenic
Basal sediments
Pre-industrial
Post-industrial
Surface sediments
PAH C#2
PAH C#1
0.0
0.1
0.2
0.3
0.4
0.5
0.6
0.7
0.8
0.9
BaA/(BaA+Chr)

Figure 7

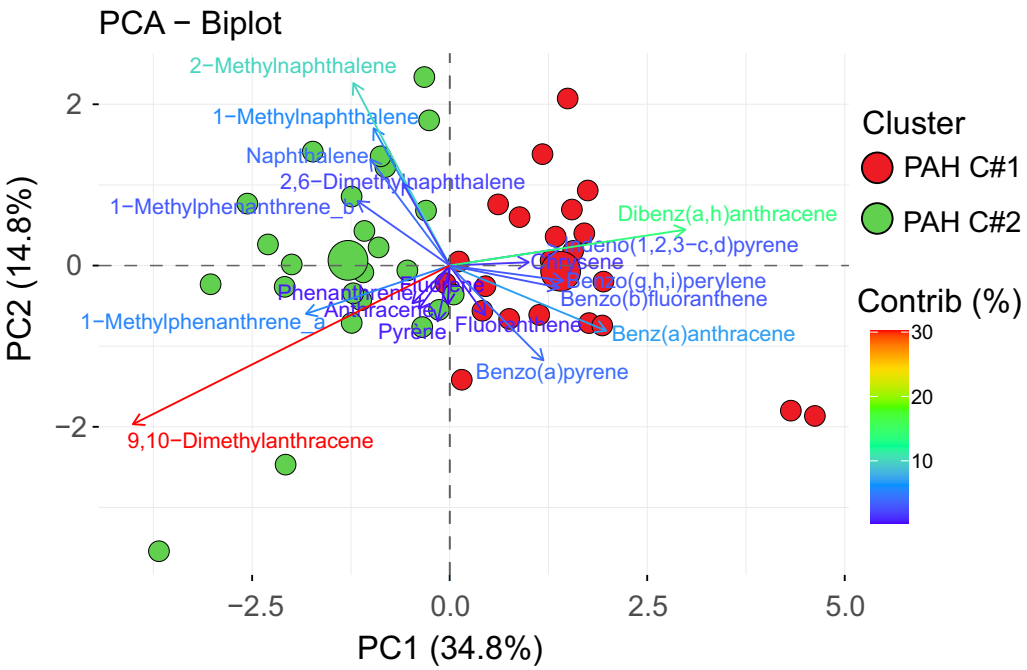
PCA − Biplot
2−Methylnaphthalene
1−Methylnaphthalene
Naphthalene
2,6−Dimethylnaphthalene
1−Methylphenanthrene_b
Dibenz(a,h)anthracene
Indeno(1,2,3−c,d)pyrene
Chrysene
Benzo(g,h,i)perylene
Benzo(b)fluoranthene
Phenanthrene
Fluorene
Anthracene
1−Methylphenanthrene_a
Pyrene
Fluoranthene
Benz(a)anthracene
Benzo(a)pyrene
9,10−Dimethylanthracene
Cluster
PAH C#1
PAH C#2
Contrib (%)
30
20
10
2
0
−2
−2.5
0.0
2.5
5.0
PC2 (14.8%)
PC1 (34.8%)

Table 1. Comparison of the ΣPAH values in EGSL marine sediments, as well as those in the sediments of other regions of the St. Lawrence River hydrological basin and worldwide river and estuarine sediments. SLE = St. Lawrence Estuary. [a] The mean value, if available, is reported in parentheses. * Only the median value is available.

Region	Number of PAHs analyzed	Values[a] (ng g^{-1})	Reference
San Joaquin River (USA)	Σ16 EPA	5 – 756 (160)	Pereira *et al.,* 1996
Boston Harbor (USA)	Σ14	483 – 718 364 (50 990)	Shiaris and Jambard-Sweet, 1986
Pearl River Delta (China)	Σ16 EPA	156 – 10 811 (2 056)	Mai *et al.,* 2002
Owen Sound Bay (Lake Huron, Great Lakes, Canada)	Σ16 EPA	85 – 46 499 (7243)	Buell *et al.,* 2021
Montréal Harbor	Σ12	14 200*	Government of Canada, 1994
Stn. 23 (head of the Lower SLE) Stn. 20 (Lower SLE/Gulf)	Σ15	238 – 351 (260) 51 – 131 (82)	Panetta, 2009
Saguenay Fjord (SLE tributary) Lower SLE	Σ12 Σ12	200 – 22 000 700 – 5 000	Gearing *et al.,* 1994
Saguenay Fjord, SLE tributary	Σ18	213 – 496	Pelletier *et al.,* 2009
Baie des Anglais (Lower SLE, near Baie-Comeau)	Σ16 EPA	373 – 38 483	Lee *et al.,* 1999
SLE – PAH C#1 SLE – PAH C#2 SLE – core sediments	Σ16 EPA Σ16 EPA Σ16 EPA	247 – 5672 (835) 72 – 2018 (353) 93 – 1621 (498)	This study

Table 2. Estimated age (common era, CE) of the basal core samples based on the sedimentation rates estimated by Smith and Schafer (1999) for nearby sediment cores, as well as their Σ_{16}PAH concentrations. The bold dates indicate the pos-tindustrial samples.

Core from this study and their analyzed depth AMD18-OSL-	**Sedimentation rate calculated by Smith and Schafer (1999) (cm yr^{-1})**	**Estimated year for the base of our cores (CE)**	**Σ_{16} PAHs (ng g^{-1})**
01BC (43-44cm)	0.539	**~ 1937**	1215.9
02BC (43-44cm)	0.580	**~ 1943**	1621.2
03BC (48-49cm)	0.248	~ 1822	147.8
05BC (42-43cm)	0.042	~ 1006	92.6
06BC (35-36cm)	0.150	~ 1781	171.9
07BC (43-44cm)	0.115	~ 1640	135.0
08BC (44-45cm)	0.139	~ 1698	103.5

Table 3. Risk assessment of the PAHs in the sediments retrieved from the study area. The red values indicate detected PAH levels that are higher than the ERL values. *The ERL and ERM values are obtained from Long et al. (1995).

Compound	Content range (ng g^{-1} dw)		ERL*	ERM*
	Surface sediments	Basal sediments		
Naphthalene	2.1 – 33.9	4.3 – 55.0	160	2100
2-Methylnaphthalene	< 17.2	< 17.2	70	670
Acenaphthylene	< 31.2	< 31.2	44	640
Acenaphthene	< 15.8 – 36.0	< 15.8	16	500
Fluorene	< 3.0 – 57.1	< 3.0 – 22.1	19	540
Phenanthrene	< 2.6 – 314.5	9.9 – 144.3	240	1500
Anthracene	< 2.6 – 73.6	< 2.6 – 27.7	85.3	1100
Fluoranthene	3.4 – 520.0	2.0 – 283.0	600	5100
Pyrene	8.8 – 700.2	6.0 – 294.1	665	2600
Benz(a)anthracene	< 1.6 – 254.3	< 1.6 – 48.3	261	1600
Chrysene	4.9 – 315.6	2.1 – 67.4	384	2800
Benzo(a)pyrene	3.4 – 664.6	0.3 – 95.8	430	1600
Dibenz(a,h)anthracene	< 3.0 – 210.4	< 3.0 – 24.2	63.4	260